Health-Monitoring of the new Benicia-Martinez Bridge - Instrumentation Plan and Preliminary Results

Carlos Zuritz & Y. H. Chai
Dept of Civil & Environmental Engineering, University of California, Davis

Li-Hong Sheng & Ganapathy Murugesh
California Department of Transportation, Sacramento, California

Hans Strandgaard
CH2M HILL, Sacramento, California

Karen Cormier
TY Lin International, San Francisco, California

ABSTRACT
This paper provides a background on the use of lightweight concrete for long span bridges. Past observations of time-dependent deflection of long-span lightweight concrete box-girder bridges are highlighted. The paper also summarizes the instrumentation program for health-monitoring of the new Benicia-Martinez Bridge, which is currently under construction in Northern California. Short and long-term service performances of the bridge are assessed through deformation measurement of the superstructure, corrosion of pile casings, temperature distribution and acoustic sensing for possible fracture of prestressing tendons. Initial field data is presented in this paper. A primary objective of the instrumentation program is to identify time-dependent effects due to creep and shrinkage for future design and analysis of long span bridges constructed of high strength lightweight concrete.

Keywords – Health monitoring, lightweight concrete, single-cell box-girder

INTRODUCTION
The new Benicia-Martinez Bridge, with a total length of over 2.5 km (1.6 miles), is one of the major lifeline structures currently under construction in northern California. The bridge is designed to accommodate five 3.6 m (12 ft) wide traffic lanes plus two 3 m (9.8 ft) wide shoulders and carry the northbound Interstate 680 traffic over the Carquinez Strait. The alignment of the new bridge will be east of the existing Benicia-Martinez Bridge and the existing Union Pacific Railroad Bridge. Some key features of the bridge include its large single-cell box-girder spans with rib-supported deck overhangs with girder depths ranging from 4.6 m (15.1 ft) to 11.5 m (37.7 ft). The bridge will include near mid-span hinges with one moment transferring hinge located on a 180.9 m (593.5 ft) long span. Also a cast-in-place balanced cantilever segmental technique was selected for the construction of the superstructure requiring post-tensioning of cast segments at early ages (Murugesh 2001).

Another key feature of the new Benicia-Martinez Bridge is the use of sand-lightweight concrete for the superstructure. The use of lightweight concrete for bridge construction is not a new development in California. Lightweight concrete has been used, for bridges as deck replacement

and rehabilitation, in regions where local aggregates are not suitable for concrete, or as a cost-effective material for long span superstructures (Caltrans 1986, Roberts 1992). Lightweight concrete also offers cost savings, particularly when used for the superstructure since the self-weight and hence the lateral inertia force is reduced.

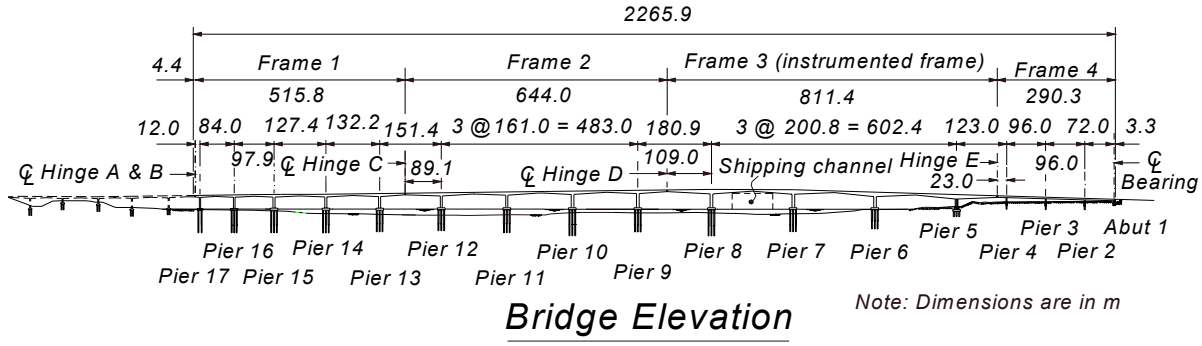

Figure 1. Elevation of the new Benicia-Martinez Bridge

Lightweight concrete has been used successfully in numerous bridge projects in California. For example, the roadway deck of the existing San Francisco-Oakland Bay Bridge was constructed of expanded shale lightweight concrete and has performed satisfactorily since 1936. Another successful example is the Napa River Bridge, a prestressed concrete bridge completed in 1977 using expanded shale (TY Lin International 1985). The Napa River Bridge has been successfully in service for over twenty years.

There have also been instances where unexpected deformation was observed during the service life of the structure constructed of lightweight concrete. For example, the Parrotts Ferry Bridge near Vallecito in California experienced a large deflection of 0.67 m (26.4 in) at mid-span after about 12 years of service The bridge, completed in May 1979, was at the time the longest three-span concrete box-girder bridge in America. Lightweight concrete was used for the single-cell box-girder superstructure and normal weight concrete was used for the substructure. The main span of the Parrotts Ferry Bridge was 195 m (640 ft), considerably longer than the 76 m (249 ft) span of the Napa River Bridge. A deflection of 0.275 m (10.8 in) was measured at mid-span about 8 months after the completion of the bridge. The deflection continued to increase at an average rate of about 0.05 m (2 in) per year for the first 6 years, followed by a reduced average rate of about 0.025 m (1 in) per year for the next 6 years. The large mid-span deflection affected the general appearance of the bridge and the sight distance of vehicles traveling on the bridge and raised concerns regarding its structural integrity.

The unexpected time-dependent deformation of the Parrotts Ferry Bridge hampered the acceptance of lightweight concrete as a suitable structural material for long-span bridge construction for many years in California. The new Benicia-Martinez Bridge is the first major lightweight concrete bridge in California since the completion of the Parrotts Ferry Bridge. Figure 1 shows an elevation of the new Benicia-Martinez Bridge where the longest span (200.8 m or 659 ft) occurs in Frame 3 over the shipping channel. Although design assumptions and details of the bridge are different from that of the Parrotts Ferry Bridge, there are nonetheless concerns regarding the potentially large span deflection of the new bridge especially considering the combination of key features of the new bridge. Prompted by these concerns, and the general lack of field data for the behavior of box-girder bridges constructed using high strength lightweight concrete and the need to forecast future condition of the bridge, a health monitoring plan is put in place to monitor the short and long term behavior of the bridge under service loads. The health monitoring program is a part of a larger instrumentation plan which includes monitoring of the bridge for extreme seismic events. The overall bid price for the health monitoring system of the new Benicia Martinez bridge, not including the cost of the instruments, was 2.5 million dollars.

PROPERTIES OF LIGHTWEIGHT CONCRETE

Although creep and shrinkage of concrete has long been recognized as an important factor influencing the distribution of internal forces such as bending moment, shear force, prestressing forces etc, actual characterization of such effects have been limited particularly for high strength lightweight concrete long-span bridges. As a result, the instrumentation program for the new Benicia-Martinez Bridge assumes special importance for the owner, researchers and practicing engineers at large.

To ensure satisfactory performance of lightweight concrete bridges, an accurate characterization of the basic properties and time dependent behavior of the concrete is important. Structural lightweight concrete must be considered as a structural material with different mechanical, thermal and chemical properties from the normal weight concrete. Table 1 compares the basic properties of normal weight concrete with that of expanded shale lightweight concrete reported in the literature (Fulginiti 1996) as well as the measured properties of the lightweight concrete used on the new Benicia-Martinez Bridge.

Table 1. Properties of normal and lightweight concrete.

Properties	Normal weight concrete	Expanded shale lightweight concrete (reported by Fulginiti 1996)	Measured high-strength lightweight concrete properties for the new Benicia- Martinez Bridge
Unit weight	22.8 – 23.6 kN/m^3 (145 – 150 lb/ft^3)	11.0 – 18.8 kN/m^3 (70 – 120 lb/ft^3)	19.5 – 19.8 kN/m^3 (124 – 126 lb/ft^3)
Compressive strength	17.2 – 138 MPa (2.5 – 20.0 ksi)	17.2 – 75.8 MPa (2.5 – 11.0 ksi)	75.8 – 77.2 MPa (11.0 – 11.2 ksi)
Tensile strength	100%	70 – 100% of tensile strength of normal weight concrete	Not available
Elastic modulus	27.6 GPa (4000 ksi) (assumed $f_c' =$ 35 MPa or 5 ksi)	20.0 GPa (2900 ksi) (assumed $f_c' =$ 35 MPa or 5 ksi)	26.2 GPa (3800 ksi) (with an $f_c' =$ 75.2 MPa or 10.9 ksi)

An important parameter governing the deformation of long span bridges is the modulus of elasticity E_c which is generally recognized as a function of the unit weight and compressive strength of the concrete. For example, ACI 318 (1999) permits the estimation of the modulus of elasticity by:

$$E_c = w_c^{1.5} 33\sqrt{f_c'} \qquad (1)$$

where f_c' = compressive strength of the concrete in psi at 28 days, and w_c = unit weight of the concrete in lb/ft^3 unit with values between 90 and 155 lb/ft^3 (14.1 and 24.3 kN/m^3). The value of E_c in Table 1 has been calculated using a compressive strength of f_c' = 34.5 MPa (5 ksi), and a unit weight of 22.5 and 18.0 kN/m^3 (143 and 115 lbs/ft^3) for normal weight and expanded shale lightweight concrete, respectively. The value of E_c for the new Benicia-Martinez Bridge is measured from concrete cylinder tests. Although the modulus of elasticity of the expanded shale lightweight concrete is expected to be about 28% lower than that of normal weight concrete, the modulus of elasticity for the lightweight concrete of the Benicia-Marinez (26 GPa or 3800 ksi) is only slightly lower than that of the normal weight concrete because of the higher compressive strength of the concrete. The 28-day compressive strength of the lightweight concrete for the new Benicia-Martinez Bridge varies between 75.8 to 77.2 MPa (11.0 to 11.2 ksi). It should be noted that Eq. 1 has been known to over-estimate the elastic modulus of high-strength lightweight concrete. Experimental data by Khaloo & Kim (1999) indicated that the Eq. 1 over-predicted the elastic modulus of high-strength lightweight concrete by 28% for a compressive strength of 77

MPa (11.2 ksi). Since the deflection of bridge structures under service loads is proportional to the modulus of elasticity, the increase in the deflection of a bridge constructed of lightweight concrete can be expected to be proportionally larger than that of normal weight concrete. Thus member size and geometry must be adjusted accordingly to account for the lower material stiffness.

INSTRUMENTATION PROGRAM

Although modest in scope, the health monitoring program of the new Benicia-Martinez Bridge is aimed at providing a better understanding of the service performance of the bridge. The long-span region of the bridge, namely Frame 3 in Figure 1, is selected for instrumentation due to its longer spans. Table 2 summarizes the number, types and date of installation of sensors on the new Benicia-Martinez Bridge, which include vertical and axial deformations of the superstructure, temperature distribution in the box-girder, corrosion potential in the pile-casings and reinforcement, forces in the prestressing tendons and hinge bearings, and potential fracture of the prestressing tendons. Field data are recorded during construction and will be continuously logged by an automated data-acquisition system for each completed instrumented region of the bridge. Display and access of real-time data will be made through high-speed internet connection.

Vertical Deflection and Axial Shortening of Spans and Rotations

Span 7, which is 200.8 m (659 ft) long over the shipping channel, is selected for vertical deformation measurement. A total of 5 displacements will be taken with measurements at every fifth point and at mid-span. A 16-gage (diameter = 1.29 mm or 0.05 in) stainless steel piano-wire, serving as a reference line for span deflection, will be tensioned between Piers 7 and 8. The piano wire will be stressed over a pulley that is attached to the diaphragm wall of Pier 7. Linear variable displacement transducers (LVDTs) will be attached to the piano-wire by feeding the wire through a hole drilled in the armature tip of the transducer. The base of the displacement transducer will be attached to the underside of the top slab along the centerline of the bridge using anchor bolts. A similar system of targeting displacement transducers on a tensioned wire for span deflection measurement has been successfully used on the North Halawa Valley Viaduct in Hawaii (Shushkewich et al 1998). The measured vertical deflections will subsequently be compared with the prediction by analysis software used during the design of the bridge.

Axial shortening of the superstructure span due to prestressing, creep and shrinkage of concrete will be measured for Span 7 and a portion of Span 8 between Pier 8 and Hinge D. An extensometer, fabricated from 6.4 mm (0.3 in) diameter Invar rods with a displacement transducer attached at one end, will be used to measure the shortening of the span. The armature tip of the transducer will be threaded into the free-end of the Invar rod. The extensometer for span shortening will be mounted on the underside of the box-girder along the centerline of the bridge, which for Span 7 will be next to the tensioned piano-wire. The Invar rod is free to slide inside a 27 mm (1.1 in) diameter PVC pipe which is suspended from the underside of the top slab of the box-girder.

Rotations of the superstructure and substructure are measured at three locations, namely at the top of the footing for Pier 7, at the pier-table of Pier 7, and at Segment 1N of Span 8. Uniaxial tiltmeters with an operating range of $\pm 5^{\circ}$ are used to measure the footing, pier-table and near-support span rotations. The tiltmeters will be mounted on a steel plate firmly bolted to the concrete surface, reaching verticality through leveling nuts.

Concrete Strains in Superstructure and Piers

Concrete strains in the superstructure will be measured using vibrating wire strain gages. A total of 40 gages will be installed at 4 cross-sections, which are located in the first segment (1N) of Span 7 and 8, and at closure pour and Hinge D of Span 8. Ten gages are used for each cross-section, as distributed according to Figure 2. Gages for span 8 segment 1N have been installed as of to-date. The distribution of strain gages will allow determination of section curvature and axial strain at the centroid of cross-section. The strain gages will also measure any non-uniform distribution of strains along the top flange of the box-girder due to shear-lag effects.

Three piers of Frame 3, namely Piers 6, 7 and 8, are also selected for concrete strain measurements. These piers are constructed using normal weight concrete. Concrete strains are measured at the base of the pier with an objective of recording the strain history due to the increasing weight of the superstructure as the balanced cantilever construction proceeds. The increase in strain may also enable the actual weight of the superstructure to be estimated.

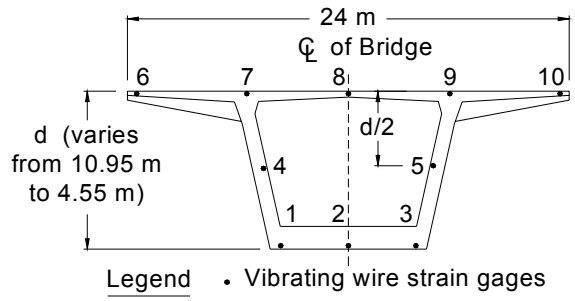

Figure 2. Distribution of vibrating wire strain gages for superstructure deformation

Corrosion of Pile Casing and Footing and Pier Reinforcement

The foundation system for the new Benicia-Martinez Bridge is supported on 2.5 m (8.2 ft) diameter steel casings filled with normal weight concrete. The thickness of the pile casing is 41 mm (1.6 in). Since steel casings are exposed to salt water, the corrosion potential of the steel casing is measured as a part of the health-monitoring program. In this case, silver/silver chloride-based corrosion cells are installed on the steel casings. Figure 3(a) shows the location of the corrosion cells on the pile casings where 4 piles in Piers 7 and 8 are selected for measurement. These cells are magnetically mounted on the outside surface of the casing at a distance 1 m (3.3 ft) below the bottom of the footing. The high side of the corrosion potential will be sensing the corrosion cell while the low side of the corrosion potential will be sensing the steel casing attached at a distance of not less than 460 mm (18.1 in) from the corrosion cell.

The corrosion potential of the footing and pier reinforcement will be measured using a silver/silver chloride based reference cell and a polarization probe. Figure 3(b) shows the corrosion cell layout for footing and pier reinforcement. The outermost reinforcement on the face of the footing is selected for monitoring of corrosion. In that location the reference cell and polarization probe are positioned center with respect to the reinforcement grid. A gap of 50 mm (2 in) is maintained between the corrosion reference cell and polarization probe. Since epoxy-coated bars are used for the footing, the attachment of the lead wire requires first removal of the coating for caldwelding followed by re-coating of the connection with epoxy. A 10-ohm resistor is placed between the high signal from the polarization probe and the low signal from the corrosion reference cell. The corrosion potential from the pair of reference cell and polarization probe is read as a differential channel by the data-acquisition system.

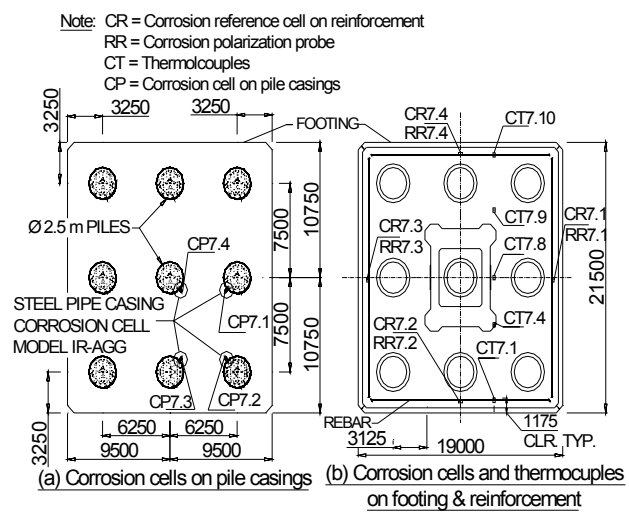

Figure 3. Corrosion cells and thermocouples in piles and pile-cap

Temperature Distributions

For adequate interpretation of measured strains and deformations, thermal effects must be considered. Temperature measurements are thus taken as a part of the health monitoring program. In addition to the correlation with strains, temperature gradients are also of interest in design since most of the design temperature distributions are proposed on the basis of normal weight concrete. Although little information existed for the temperature distribution of large single cell box-girder bridges during the design of the new Benicia-Martinez Bridge, it is well known that structural

lightweight concrete has lower thermal conductivity and lower thermal coefficient of expansion compared to that of normal weight concrete (ACI 213-R79 1984). The lower thermal conductivity results in smaller temperature changes in the interior portion of the structure during a transient temperature variation, while the lower thermal coefficient of expansion results in smaller deformation and thermally-induced forces. In this project, temperature distributions are measured using Teflon-insulated copper/constantan thermocouples in the footing of Pier 7 and at two sections of the superstructure in Span 7. Ten thermocouples are used in the footing, as shown in Figure 3(b) where the symbol CT denotes the thermocouple location. Two sections located in the first segment of Span 7 and in the closure pour of Span 7 are selected for temperature measurement. Twenty thermocouples are used on sensing the temperature distribution in each section. Air temperature and relative humidity inside and outside of the box-girder will also be measured as part of the instrumentation program since these parameters will also influence the creep and shrinkage of the concrete. Internal air temperature and outside relative humidity will be measured at the pier table of Pier 7 while the external air temperature and inside relative humidity will be measured at closure pour of Span 7.

Prestressing Tendons and Hinge Bearing Forces

Two of the prestressing tendons in Span 7 will be monitored with center-hole loadcells. The loadcells are located in Segment 12N of Span 7 (about one-quarter span) and in the closure pour of Span 7. Loadcells for the prestressing tendons are inserted between the anchor plate for the prestressing wedges and the bearing plate on the concrete. Measured tendon forces will allow the determination of the actual tendon relaxation over time. The tendons will remain ungrouted during the monitoring period. Eight bearings in Hinge D of Span 7 will also be instrumented with loadcells. Measured forces in the loadcells of the bearings will enable a characterization of the moment redistribution over time as a result of time-dependent effects.

Monitoring of Prestressing Tendons for Fracture

Although fracturing of prestressing tendons is not expected during the initial service life of the bridge, corrosion or redistribution of internal forces due to time-dependent effects or high-cycle fatigue due to repeated cycles under long-term service loads may lead to failure of the tendons. As a part of the health-monitoring of the bridge, an acoustic sensing system developed by Pure Technologies Ltd. has been proposed to monitor the prestressing tendons on a portion of the bridge. The acoustic sensing system utilizes a grid of sensors (broadband accelerometers) to detect signals generated by the tendon fracture. Techniques have been developed to detect signals above the ambient noise level and to enable the location of fracture in the tendon to be identified. A total of 84 sensors will be installed in Span 8 between Pier 8 and Hinge D. Twelve cross-sections at spacing of 9.6 m (31.5 ft) are instrumented with 7 sensors provided for each section.

PRELIMINARY RESULTS

Data is being recorded during the construction of the bridge and is available at the time of writing this paper. In terms of construction, Pier 8 is the most advanced among the three piers of the instrumented frame, and consequently, the largest set of data was derived from this pier. Acquired data to-date includes corrosion cell potential on pile casings, footing and pier reinforcement as well as concrete strains at the base of the pier and in segment 1N of Span 8. At this time, measured corrosion cell potential does not indicate on-set of corrosion in the reinforcement or pile-casing as expected for the short service life of the structure, and will therefore not be presented. Structural deformation data recorded up to this stage of construction are presented.

Measured Concrete Strains at the Base of Pier 8

Strain history as measured at the base of the Pier 8 i.e. top of the footing is plotted for one of the gages (VWSG 8.3) in Figure 4. The gage is located on inside face of the pier, which has a hollow cross-section with a wall thickness of 0.75 m (29 in) in the northern and southern wall. Strain variation is plotted for two complete casting cycles i.e. a total of 4 segments (8-8N, 8-8S, 8-9N and 8-9S) were added to the superstructure in 17 days. The plot of compressive strain is used to

illustrate the variation of strain expected of the concrete due to the increased number of cast segments.

The line corresponding to total strain ε_{total} in Figure 4 represents the strain measured by the vibrating wire strain gage. The variation is seen to follow the expected trend in a cast-in-place balanced cantilever segmental construction. The strain history is characterized by a small daily temperature fluctuation and a large strain increment as a result of the addition of the new segments. The strain variation for ε_{total} due to the daily temperature cycle is of the order of 20×10^{-6} while the change due to the addition of a new segment is of the order of 40×10^{-6}. As can be observed in the figure, the addition of the north segments i.e. 8-8N and 8-9N produces an increase in compressive strains while the addition of the south segments i.e. 8-8S and 8-9S produces a corresponding decrease in compressive strains. This strain history is expected for cast-in-place balanced cantilever segmental construction.

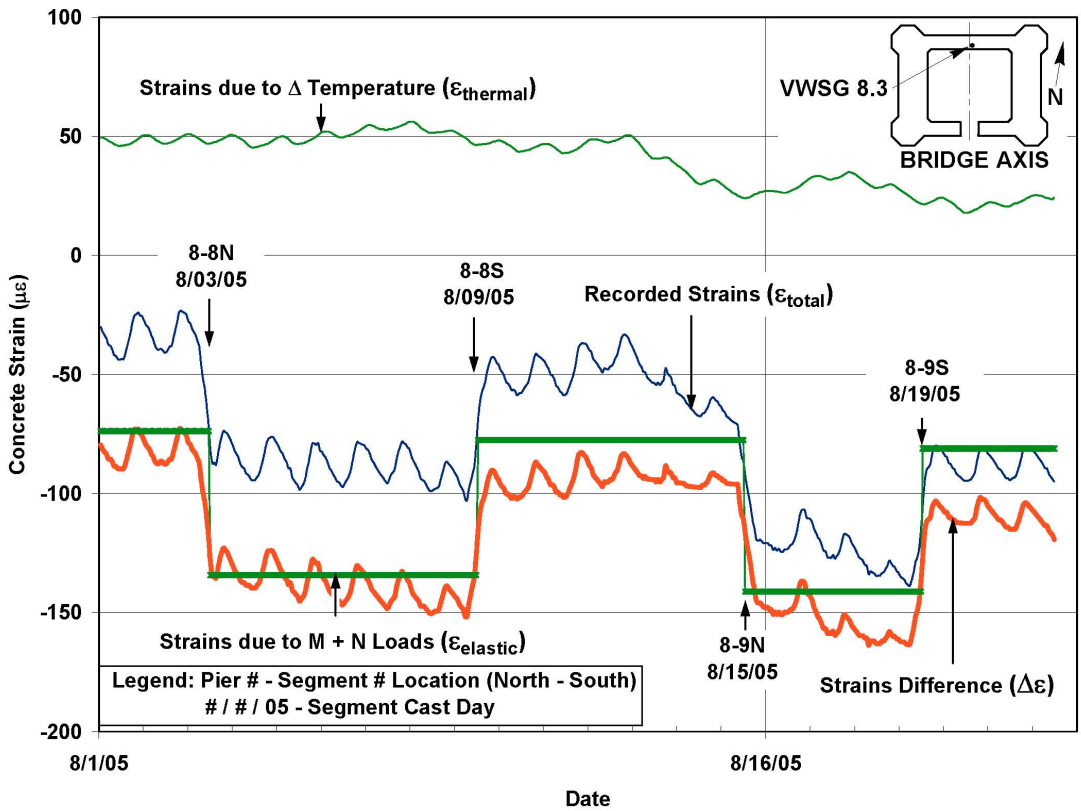

Figure 4. Strains at Base of Northern Inner Face Wall of Pier 8.

Also shown in Figure 4 is the thermal strain $\varepsilon_{thermal}$ variation with time as determined by the product of thermal coefficient of expansion (assumed to be 10.8×10^{-6} /°C) and the temperature change. A strain variation of approximately 8×10^{-6} is noted for $\varepsilon_{thermal}$ for a typical daily temperature cycle, or equivalently a 0.7°C change in temperature. It is apparent, upon comparison of the total strain and thermal strain, that the range of daily strain variation for ε_{total} and $\varepsilon_{thermal}$ are not similar (20×10^{-6} for ε_{total} versus 8×10^{-6} for $\varepsilon_{thermal}$). The temperature, measured by the thermistor in the vibrating wire strain gage, is relatively constant in the interior portion of the pier wall while the exterior portion of the pier wall is expected to undergo a larger variation in temperature through the daily cycle. The temperature difference between the exterior and interior portions of the pier wall is likely to result in a nonlinear temperature distribution across the wall thickness. Strain compatibility across the pier section imposes tension in the interior region of the pier when the exterior temperature is higher than the interior temperature. The converse would be

true when the exterior temperature of the pier wall is lower than the interior temperature. The difference in strain between ε_{total} and $\varepsilon_{thermal}$ may therefore be attributed to the thermally induced stress that maintains strain compatibility across the wall section. Although not presented at this time, the recorded strain history shows small tensile strains in the interior face of the northern pier wall, which is unexpected under the self-weight condition. This phenomenon will be further analyzed by analytical models to determine the magnitude of these strains and their importance once compared to the limits imposed by the design codes.

The difference between the total strain and thermal strain, denoted as $\Delta\varepsilon = \varepsilon_{total} - \varepsilon_{thermal}$, is also plotted in Figure 4. The strain difference $\Delta\varepsilon$ can be compared to the 'elastic' strain $\varepsilon_{elastic}$ due to the axial compression and out-of-balance moment from the self-weight of the pier and superstructure. The elastic strain $\varepsilon_{elastic}$ is estimated using the modulus of elasticity for the pier base normal weight concrete at age of approximately 400 days i.e. 30 GPa (4351 ksi). The estimated elastic strain $\varepsilon_{elastic}$ is plotted as a constant value in Figure 4 for each casting interval. As observed in Figure 4, the elastic strain $\varepsilon_{elastic}$ compares very well with the strain difference $\Delta\varepsilon$ implying that the time-dependent strains are of smaller magnitude at this time of health monitoring.

Measured Concrete Strains in Segment 1N of Span 8

Concrete strains (in the direction of the bridge axis) in the south section of segment 1N have been logged for 91 days. The strain data measured by ten vibrating wire strain gages, with location indicated in Figure 2, are presented as strain profiles in Figures 5 and 6. It should be noted that the strains plotted are not peak strains but rather strains measured at 10 am soon after the completion of the longitudinal post-tensioning of the segments. In Figure 5, the strains are plotted as distributions across the top flange, whereas in Figure 6, the strains are plotted along the depth of the cross-section. For both figures, differentiation is made with regard the post-tensioning sequence. Strain profiles after post-tensioning a north segment are indicated by solid lines while the profiles after post-tensioning a south segment are indicated by dashed lines. A total of 11 strain profiles each corresponding to the post-tensioning of alternating segments (2N and 2S through 7N) is presented.

It can be seen from Figure 5 that the strain profile across the top flange (as measured by 5 gages) is not uniform. For the first segment shown as 2N, the strains measured in the overhang portion of the box-girder are larger than the strains measured over the web portion of the flange. However, in subsequent post-tensioning of segments, the trend reverses with larger strains being measured in the web portion of the flange compared to that measured in the overhang. The compressive strain measured in the west overhang of the box-girder is also larger than the strain measured in the east overhang, indicating that there is an associated plan curvature in the box-girder. The non-symmetric strain profile across the bridge centerline may be due to the post-tensioning of segment 1N by non-symmetric loads. In this case, the jacking force on the western tendon was 4101 kN (922 kips) which was higher than the 4301 kN (967 kips) applied on the eastern tendon. The non-symmetric strain profile may also be augmented by the higher temperature exposure to the morning sun by the east overhang, which causes a tensile strain and thus relieves the compressive strain due to the post-tensioning.

The cast-in-place balanced cantilever segmental construction also has an interesting influence on the measured concrete strains in the superstructure. In general, the casting and post-tensioning of north segments induce a positive change in the strains measured in segment 1N. The positive change in strain is due to the moment from the self-weight of the new segment. In contrast, the strain change from casting and post-tensioning of south segments is negative since the measured strains in segment 1N are only influenced by the compressive force from the post-tensioning. This effect can be seen by comparison of the strain profiles for north segment with that of south segments e.g. 3N versus 3S in Figure 5.

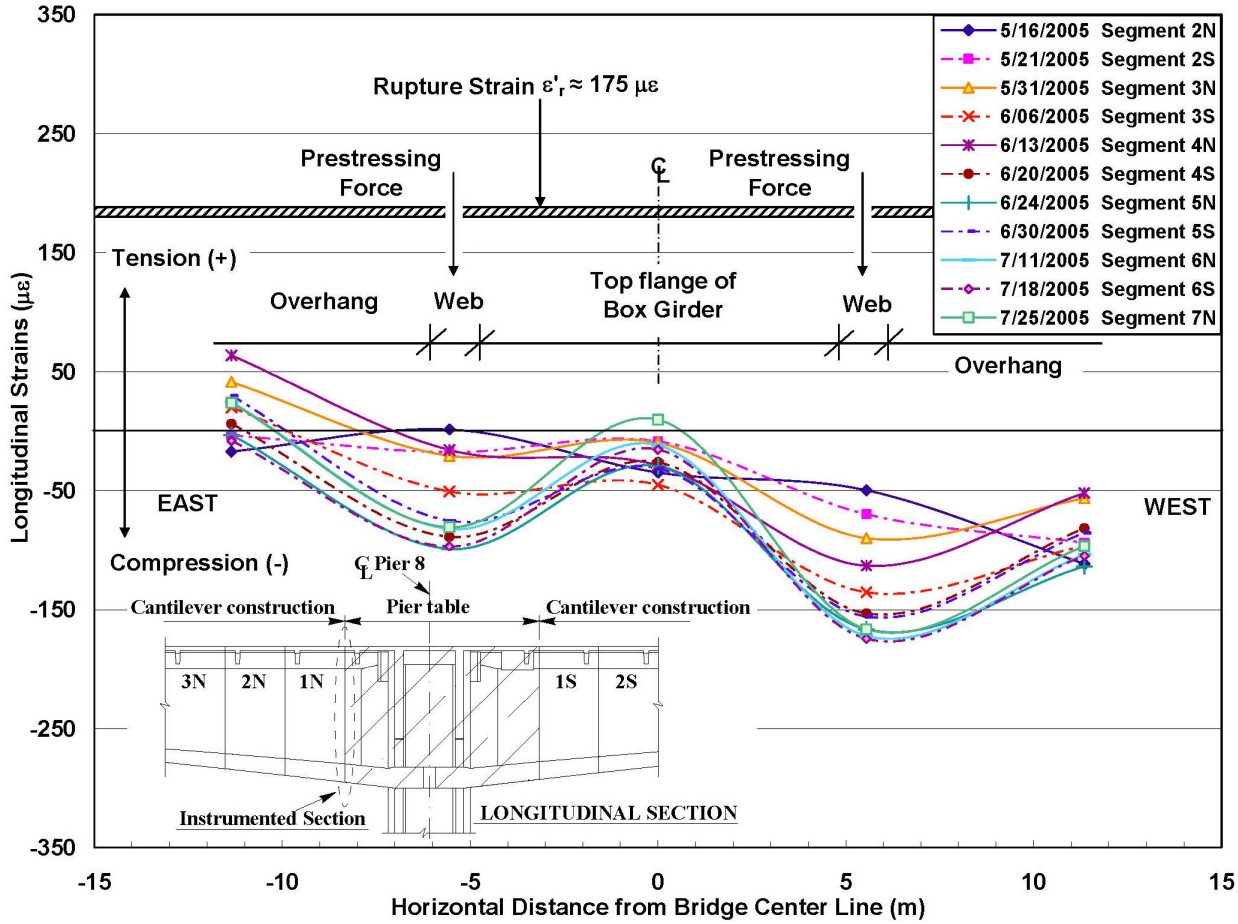

Figure 5. Longitudinal concrete strain distribution across the flange and overhangs of the box-girder (Segment 1N of Span 8).

Note that the plot of strain profiles in Figure 5 show a maximum tensile strain of about 50×10^{-6} in the top flange, for measurement taken at 10 am. The tensile strain is small compared to the rupture strain of the concrete, which is indicated by a thick hatch line in the upper region of Figure 5. The rupture strain of 173×10^{-6} is estimated from the modulus of rupture f_r' in psi, which is assumed to be related to the compressive strength f_c' in psi, by $f_r' = 6.3\left(f_c'\right)^{1/2}$ as given by the current Caltrans Bridge Design Specifications (2005). A value of f_c' = 75 MPa (10.9 ksi) and E_c = 26.22 GPa (3803 ksi), obtained from averaged field specimens of the superstructure lightweight concrete. Although not plotted in Figure 5, peak tensile strains recorded throughout the entire history are smaller than the estimated rupture indicating that the superstructure should not experience cracking during construction under the specified code limits.

The longitudinal concrete strains along the depth of the south section of segment 1N are plotted in Figure 6. It should be noted that the strain plotted at the top corresponds to the average strain of the 5 strain gages across the flange, whereas the strain at mid-height corresponds to the average of two strain gages and the strain at the soffit corresponds to the average strain of two strain gages (one of the three gages did not have the correct reference strain value). It can be seen from the figure that the strain in the top flange is compressive whereas the strain in the soffit is tensile.

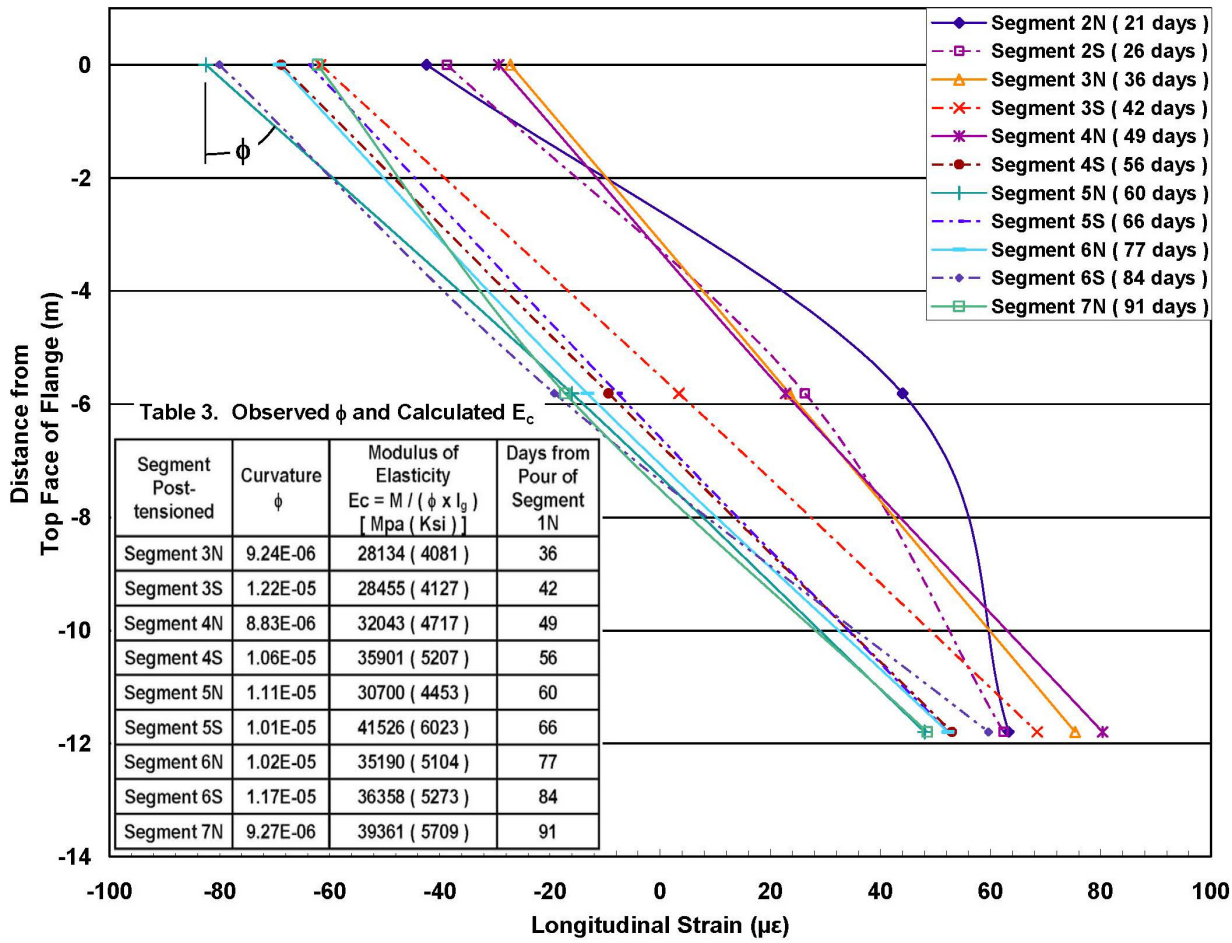

Table 3. Observed ϕ and Calculated E_c

Segment Post-tensioned	Curvature ϕ	Modulus of Elasticity Ec = M / (ϕ x I_g) [Mpa (Ksi)]	Days from Pour of Segment 1N
Segment 3N	9.24E-06	28134 (4081)	36
Segment 3S	1.22E-05	28455 (4127)	42
Segment 4N	8.83E-06	32043 (4717)	49
Segment 4S	1.06E-05	35901 (5207)	56
Segment 5N	1.11E-05	30700 (4453)	60
Segment 5S	1.01E-05	41526 (6023)	66
Segment 6N	1.02E-05	35190 (5104)	77
Segment 6S	1.17E-05	36358 (5273)	84
Segment 7N	9.27E-06	39361 (5709)	91

Figure 6. Longitudinal concrete strain distribution along the depth of the of the cross-section (Segment 1N of Span 8).

This is expected since the effect of the post-tensioning force is larger that of the negative moment from the self-weight of the added segments. Initially the measured strains indicated a nonlinear profile along the depth, as signified by the lines for 2N and 2S. However, with increasing number of segments, the strain profiles become almost linear indicating that kinematic assumption for beam flexure, i.e. plane sections before bending remain plane, holds for the large single-cell box-girder of the new Benicia-Martinez Bridge. The linearity of the strain profiles allows for an estimation of curvature ϕ and its evolution after the post-tensioning of each segment. Since the bending moment acting on the section M can be estimated from the self-weight of the segment, the 'effective' elastic modulus E_c^{eff} can be calculated from the best-fit measured curvature ϕ and the gross moment of inertia of the section I_g:

$$E_c^{eff} = \frac{M}{\phi \cdot I_g} \tag{3}$$

The effective elastic moduli at different ages are given in the table in Figure 6. The effective elastic modulus varies from about 26 GPa (3800 ksi) to 40 GPa (5800 ksi) with larger modulus being observed at later age. These values are higher than the elastic modulus from on-site cylinder compression tests and the values used in the design of the bridge.

CONCLUSIONS

High strength lightweight concrete has been used, or proposed for use, for bridges as deck replacement and rehabilitation, or for use in regions where local aggregates are not suitable for concrete, or as cost-effective materials for long-span construction. While a number of bridges in California have enjoyed the successful use of lightweight concrete, there were nonetheless instances where unexpectedly large time-dependent deformation of the superstructure raised concerns regarding the integrity of the bridge. This paper provides a background on the use of lightweight concrete for bridges in California. It also summarizes the instrumentation program for health monitoring of the new Benicia-Martinez Bridge, which is currently under construction in Northern California. Short and long-term service performance of the new bridge is monitored through time-dependent deformation of the superstructure, corrosion of the pile casings, temperature distribution in the superstructure box-girder, and acoustic sensing for possible fracture of prestressing tendons. Initial field data and its comparison with theoretical values are presented in this paper. Future work will consist of more detailed comparisons of measured deformation with predictions by current analytical tools including creep and shrinkage models. These data, once collected and reduced, will also be compared to current design specifications serving to advance the useful knowledge base for design of future high strength lightweight concrete structures in California and elsewhere.

REFERENCES

ACI 213R-79. 1984. Guide for structural lightweight aggregate concrete. *ACI manual of Concrete Practice, Part 1*. American Concrete Institute.

ACI 318. 1999. *Building Code Requirements for Structural Concrete* (ACI 318-99) and Commentary.

Caltrans. 1986. *Memos to Designers 21-47 - Lightweight Concrete*. Sacramento.

Caltrans. 2005. *Bridge Design Specifications – Prestressed Concrete.* Sacramento.

Dokken, R.A. 1996. Napa River Bridge – 20 years later. *International Symposium on Lightweight Concrete Bridges,* 10 September, 1996. Sacramento.

Fulginiti, J.L. 1996. Expanded shale lightweight concrete, production and development. *International Symposium on Lightweight Concrete Bridges*, September 10, 1996. Sacramento.

Khaloo, A.R. & Kim Nakseok 1999. Effects of curing condition on strength and elastic modulus of lightweight high-strength concrete. *ACI Materials Journal* 96(4): 485-490.

Mehta, P.K. 1986. *Concrete Structures, Properties, and Materials.* Prentice Hall Inc., Englewood Cliffs, NJ, pg 384.

Mindess, S., et al. 2002. *Concrete,* 2nd Edition, Prentice Hall Inc., Upper Saddle River, NJ, pp. 538.

Murugesh, G. 2001. Health Monitoring of the New Benicia Martinez Bridge. *Health Monitoring and Management of Civil Infrastructure Systems.* SPIE Proceeding 4337, 256-267.

Roberts, J.E. 1992. *Lightweight Concrete Bridges for California Highway System.* American Concrete Institute Publication SP 136, 255-271.

Shushkewich, K. W. et al. 1998. *Instrumentation of the North Halawa Valley Viaduct, Oahu, Hawaii*. Hawaii Department of Transportation and Federal Highway Administration.

T. Y. Lin International. 1985. *Criteria for designing lightweight concrete bridges*. Federal Highway Adminstration, Report No. FHWA/RD-85/045.

Table 2. Summary of instrumentation plan for the new Benicia-Martinez Bridge

Measurement	Sensor type	No.	Location	Comments	Installed
Vertical span deflections	LVDTs	5	Span 7 – 1/5, 2/5, 3/5, 4/5 and mid-span	Tensioned piano-wire as reference line	Not yet installed
Span shortening	LVDTs	2	Span 7 (200.8 m or 658.8 ft) and Span 8 between Pier 8 and Hinge D (100.9 m or 331 ft)	Use of 6.4 mm (.25 in) diameter Invar rod as extensometer	Not yet installed
Rotations	Uniaxial tiltmeters	3	Top of Pier 7 footing, underside of deck at Pier 7 table, and Segment 1 N of Span 8	Angular range of tiltmeter is $\pm 0.5^o$	8-1N: 8/27/05 Others not yet installed
Lightweight Concrete strains in superstructure	Vibrating wire strain gages (VWSGs)	40	Segment 1N – Span 7 & Span 8, and closure pour of Span 7 and Hinge D of Span 8	Ten gages per section near pier and at mid-span	8 -1N: 4/18/05 Others not yet installed
Concrete strains in pier (normal weight concrete)	Electrical resistance (ERSGs) and vibrating wire strain gages	24	Four electrical resistance strain gages and four vibrating wire strain gages per pier for Piers 6, 7 and 8. Gages installed at the base of the pier.	Electrical resistance and vibrating wire strain gages are installed as pairs on each face of the pier	Pier 6: 8/04/05 Pier 7: 1/15/05 Pier 8: 7/26/04
Corrosion of pile casings	Corrosion cells	8	One corrosion cell per casing with four instrumented casing per pier (Piers 7 and 8). Corrosion cells are mounted 1 m (3.3 ft) below the footing	Corrosion cells for casings magnetically mounted on the surface of the casing	Pier 8: 4/19/05 Pier 7: 4/21/05
Corrosion of footing and pier reinforcement	Corrosion reference cell and polarization probe	16 pairs	Four pairs of reference cells and polarization probes installed at the top of the footing and four pairs at 1 m (3.3 ft) above footing for Piers 7 and 8	Reference cells are silver/silver chloride based (Ag/Ag Cl)	Footing 8: 7/13/05 Footing 7: 1/07/05 Pier wall same date as ERSGs
Concrete temperature	Thermocouples	50	Ten thermocouples on footing of Pier 7, twenty thermocouples on Segment 1N of Pier 7 & twenty thermocouples on closure pour of Span 7	Six thermocouples on top and bottom slabs and four on webs of box-girder	Pier 7 footing: 1/07/05 Others not yet installed
Air temperature	Thermocouples	2	One internal air temperature at Pier 7 table and one external air temperature at closure pour of Span 7	External thermocouple installed on permanent shadow of deck overhang	Not yet installed
Relative humidity	Humidity meters	2	Outside relative humidity at pier table of Pier 7 and inside relative humidity at closure pour of Span 7	Exterior relative humidity accessed through a 25 mm (1 in) PVC pipe cast in the concrete wall	Not yet installed
Tendon forces and in-span hinge forces	Loadcells	10	Two tendons in Span 7 are monitored for forces & eight bearings at Hinge D are monitored for forces	Tendon forces monitored by VWSGs and bearings monitored with ERSGs	Not yet installed
Prestressing wire breakage	Acoustic sensors	84	Span 8 between Pier 8 and Hinge D (9 sections with 7 sensors per section)	Proprietary system by Pure Technologies Ltd.	Not yet installed